4. G. R. Tanner, A. Lutas, J. R. Martínez-François, G. Yellen, *J. Neurosci.* **31**, 8689–8696 (2011).
5. A. Giménez-Cassina *et al*., *Neuron* **74**, 719–730 (2012).
6. N. Juge *et al*., *Neuron* **68**, 99–112 (2010).
7. S. A. Masino *et al*., *J. Clin. Invest.* **121**, 2679–2683 (2011).
8. A. Lutas, G. Yellen, *Trends Neurosci.* **36**, 32–40 (2013).
9. B. S. Meldrum, M. A. Rogawski, *Neurotherapeutics* **4**, 18–61 (2007).
10. K. J. Bough *et al*., *Ann. Neurol.* **60**, 223–235 (2006).
11. Materials and methods are available as supplementary materials on *Science* Online.
12. D. Dybdal, K. Gale, *J. Neurosci.* **20**, 6728–6733 (2000).
13. M. J. Iadarola, K. Gale, *Science* **218**, 1237–1240 (1982).
14. I. A. Silver, M. Erecińska, *J. Neurosci.* **14**, 5068–5076 (1994).
15. Z. Song, B. E. Levin, J. J. McArdle, N. Bakhos, V. H. Routh, *Diabetes* **50**, 2673–2681 (2001).
16. M. O. Cunningham *et al*., *Proc. Natl. Acad. Sci. U.S.A.* **103**, 5597–5601 (2006).
17. M. Bélanger, I. Allaman, P. J. Magistretti, *Cell Metab.* **14**, 724–738 (2011).
18. N. Rouach, A. Koulakoff, V. Abudara, K. Willecke, C. Giaume, *Science* **322**, 1551–1555 (2008).
19. M. P. Parsons, M. Hirasawa, *J. Neurosci.* **30**, 8061–8070 (2010).
20. A. Suzuki *et al*., *Cell* **144**, 810–823 (2011).
21. H. Shimizu *et al*., *Neuron* **54**, 59–72 (2007).
22. T. K. Lam, R. Gutierrez-Juarez, A. Pocai, L. Rossetti, *Science* **309**, 943–947 (2005).
23. R. D'Ambrosio, J. Wenzel, P. A. Schwartzkroin, G. M. McKhann 2nd, D. Janigro, *J. Neurosci.* **18**, 4425–4438 (1998).
24. V. Riban *et al*., *Neuroscience* **112**, 101–111 (2002).
25. R. Samala, J. Klein, K. Borges, *Neurochem. Int.* **58**, 5–8 (2011).
26. C. Chiron *et al*., *Lancet* **356**, 1638–1642 (2000).
27. R. H. Caraballo *et al*., *Epilepsia* **46**, 1539–1544 (2005).
28. L. M. Deck *et al*., *J. Med. Chem.* **41**, 3879–3887 (1998).
29. C. Granchi *et al*., *J. Med. Chem.* **54**, 1599–1612 (2011).
30. M. K. Trojnar, K. Wojtal, M. P. Trojnar, S. J. Czuczwar, *Pharmacol. Rep.* **57**, 154–160 (2005).
31. P. P. Quilichini, C. Chiron, Y. Ben-Ari, H. Gozlan, *Epilepsia* **47**, 704–716 (2006).

ACKNOWLEDGMENTS

We thank K. Imoto for comments on this manuscript, D. Kase for technical advice on in vivo recordings at the initial stage, and A. Wakasa and K. Urakawa for their technical support on the intrahippocampal kainate model. N.S., S.L., T.O., and T.I. are inventors on a patent (World Intellectual Property Organization WO2014/115764) related to clinical use of stiripentol as LDH inhibitors, and N.S. and T.I. are also inventors on a patent (Japan JP2015-023572) related to isosafrole as antiepileptic compounds. These patent applications have been filed by Okayama University. All data described in the paper are presented in this report and supplementary materials. This work was supported by grants from the Japan Society for the Promotion of Science (24590114) and by research grants from Takeda Science Foundation and Ryobi-Teien Memory Foundation.

SUPPLEMENTARY MATERIALS

www.sciencemag.org/content/347/6228/1362/suppl/DC1
Materials and Methods
Supplementary Text
Figs. S1 to S26
References (*32*–*59*)

21 October 2014; accepted 9 February 2015
10.1126/science.aaa1299

TRANSLATION

An RNA biosensor for imaging the first round of translation from single cells to living animals

James M. Halstead,[1]* Timothée Lionnet,[2,3,4]* Johannes H. Wilbertz,[1,5]* Frank Wippich,[6]* Anne Ephrussi,[6]† Robert H. Singer,[2,3,4]† Jeffrey A. Chao[1,2]†

Analysis of single molecules in living cells has provided quantitative insights into the kinetics of fundamental biological processes; however, the dynamics of messenger RNA (mRNA) translation have yet to be addressed. We have developed a fluorescence microscopy technique that reports on the first translation events of individual mRNA molecules. This allowed us to examine the spatiotemporal regulation of translation during normal growth and stress and during *Drosophila* oocyte development. We have shown that mRNAs are not translated in the nucleus but translate within minutes after export, that sequestration within P-bodies regulates translation, and that *oskar* mRNA is not translated until it reaches the posterior pole of the oocyte. This methodology provides a framework for studying initiation of protein synthesis on single mRNAs in living cells.

During translation, mRNAs are bound by the ribosome. Measurements of ribosome occupancy of mRNAs and protein abundance provide a genome-wide view of translation regulation (*1*, *2*). Fluorescence microscopy complements these global approaches because it allows analysis of gene expression with single-molecule resolution in living cells and provides mechanistic insights obscured by ensemble measurements (*3*, *4*). Imaging methods have been developed that allow newly synthesized proteins to be discerned from the preexisting population or enable actively translating ribosomes to be identified within the cell; however, these approaches are limited by low signal-to-noise ratio and lack the resolution to correlate these events with specific mRNA molecules (*5*). Here, we describe a single-molecule assay that allows untranslated mRNAs to be distinguished unequivocally from previously translated ones and provides a foundation for investigating the spatiotemporal regulation of translation in living cells.

Because the ribosome or its associated factors must displace endogenous RNA-binding proteins during the first round of translation, we reasoned that it would be possible to construct an RNA biosensor whose fluorescent signal would depend on this process. The orthogonal bacteriophage PP7 and MS2 stem-loops were used to label a transcript within both the coding sequence (PP7) and the 3′ untranslated region (UTR) (MS2) with spectrally distinct fluorescent proteins (*6*). Simultaneous expression of the PP7 coat protein fused to a nuclear localization sequence (NLS) and green fluorescent protein (NLS-PCP-GFP) and the MS2 coat protein fused to an NLS and red fluorescent protein (NLS-MCP-RFP) resulted in nuclear transcripts labeled with both fluorescent proteins (Fig. 1A). Upon export of the reporter mRNA, the first round of translation displaces NLS-PCP-GFP from the transcript, as the ribosome traverses the coding region that contains the PP7 stem-loops. The NLS limits the concentration of free NLS-PCP-GFP in the cytoplasm, yielding translated mRNAs that are labeled with only NLS-MCP-RFP bound to the stem-loops in the 3′ UTR (Fig. 1, A and B). We refer to this technique as translating RNA imaging by coat protein knock-off (TRICK).

Efficient translation of a 6xPP7 stem-loop cassette required optimization of the distance between adjacent stem-loops, stem-loop folding, and codon usage so that they would not block or stall elongation of the ribosome, which might elicit decay of the transcript (*7*) (Fig. 1C). The polypeptide encoded by the PP7 stem-loops has a molecular mass of ~14 kD and is not homologous to any known protein. Binding of NLS-MCP-RFP to the 3′ UTR had no effect on translation, and binding of NLS-PCP-GFP to the PP7 stem-loop cassette in the coding region also did not result in reduced translation of the reporter mRNA (Fig. 1C and fig. S1). Similarly, binding of the fluorescent proteins to the reporter mRNA also did not alter the stability of the transcript (fig. S2).

The TRICK reporter mRNA was expressed in a U-2 OS human osteosarcoma cell line stably expressing NLS-PCP-GFP and NLS-MCP-RFP. Fluorescence-activated cell sorting isolated cells with small amounts of both fluorescent proteins, allowing detection of all reporter mRNAs (figs. S3 and S4). The cells were imaged on a fluorescence microscope equipped with two registered cameras, allowing simultaneous visualization of single mRNA molecules in both channels. In the nucleus, single mRNAs were fluorescently labeled with both red

[1]Friedrich Miescher Institute for Biomedical Research, CH-4058 Basel, Switzerland. [2]Department of Anatomy and Structural Biology, Albert Einstein College of Medicine, Bronx, NY 10461, USA. [3]Gruss-Lipper Biophotonics Center, Albert Einstein College of Medicine, Bronx, NY 10461, USA. [4]Transcription Imaging Consortium, Howard Hughes Medical Institute Janelia Farm Research Campus, Ashburn, VA 20147, USA. [5]University of Basel, CH-4003 Basel, Switzerland. [6]Developmental Biology Unit, European Molecular Biology Laboratory, 69117 Heidelberg, Germany.
*These authors contributed equally to this work. **†Corresponding author. E-mail: ephrussi@embl.de (A.E.); robert.singer@einstein.yu.edu (R.H.S.); jeffrey.chao@fmi.ch (J.A.C.)**

and green proteins and thus appeared yellow (Fig. 1D). In contrast, almost all of the mRNAs appeared as red particles in the cytoplasm, indicating that only NLS-MCP-RFP was bound (Fig. 1, D and E). Quantification of the steady-state number of yellow mRNAs in the cytoplasm revealed that ~94% of TRICK reporter mRNAs had been translated at least once (Fig. 1, E and H). To confirm that loss of NLS-PCP-GFP from cytoplasmic transcripts was translation-dependent, we induced transcription of the TRICK reporter by ponasterone A (ponA) in the presence of translational inhibitors (*8*). Adding either cycloheximide, which inhibits elongation, or puromycin, which causes premature termination, for 30 min before induction of TRICK reporter mRNA expression resulted in an increase in the number of untranslated mRNAs in the cytoplasm (Fig. 1, F to H, and movies S1 to S3). Consistent with the imaging, polysome analysis indicated that NLS-PCP-GFP was absent from actively translating mRNAs, whereas NLS-MCP-RFP could be detected within polysomes (fig. S5). This demonstrated that translation of the PP7 stem-loops by the ribosome was required for displacement of the green signal from the mRNA.

Although translation is thought to occur exclusively in the cytoplasm, recent studies suggest that protein synthesis can occur in the nucleus (*9*, *10*). Because the TRICK assay can distinguish between untranslated and translated mRNAs, we imaged TRICK reporter mRNAs in the nucleus 30 min after ponA induction. Single-particle tracking (SPT) of nuclear mRNAs determined that they undergo both corralled (D = 0.02 $\mu m^2\ s^{-1}$) and random diffusion (D = 0.09 $\mu m^2\ s^{-1}$), similar to the movements observed for other nuclear mRNAs (*11*, *12*). We found 91.3 ± 0.9% of mRNAs labeled with both colors, which is not significantly different from the fraction of double-labeled mRNAs in the cytoplasm of cells treated with translational inhibitors (P = 0.75, unpaired t test) (fig. S6, A and B, and movie S4). We cannot, however, exclude the possibility that the fusion protein rebound the PP7 stem-loops immediately after translation. If translation were occurring in the nucleus, addition of small amounts of cycloheximide would increase polysome formation, causing occlusion of the PP7 stem-loops and thereby preventing NLS-PCP-GFP from rebinding (*13*) (fig. S7A). Similar to experiments in the absence of cycloheximide, 90.7 ± 0.6% of nuclear mRNAs were labeled with both colors when cells were treated with 1 $\mu g\ ml^{-1}$ cycloheximide (P = 0.44, unpaired t test) (fig. S7, B and C, and movie S5). Although it is possible that nuclear translation could occur for specific mRNAs, this was not observed for the TRICK reporter. These findings are consistent with the previous observation that mRNAs containing premature stop codons are exported before undergoing decay in the cytoplasm (*14*).

The rapid diffusion of mRNAs in the cytoplasm and photobleaching prevented us from imaging a single mRNA from the time it entered the cytoplasm until it was translated (figs. S8 and S9). Untranslated mRNAs, however, could be detected after export from the nucleus and were observed throughout the cytoplasm (fig. S8). To verify these live-cell observations, we measured the spatial distribution of untranslated reporter mRNAs in fixed cells, using a combined immunofluorescence–fluorescence in situ hybridization (IF-FISH) approach. FISH probes targeted to the MS2 stem-loops allowed detection of all reporter mRNAs, whereas a GFP nanobody was used to identify the untranslated ones (fig. S10, A and B). In agreement with live-cell results, we observed a large percentage of cytoplasmic translated mRNAs (93.7%). As mRNAs

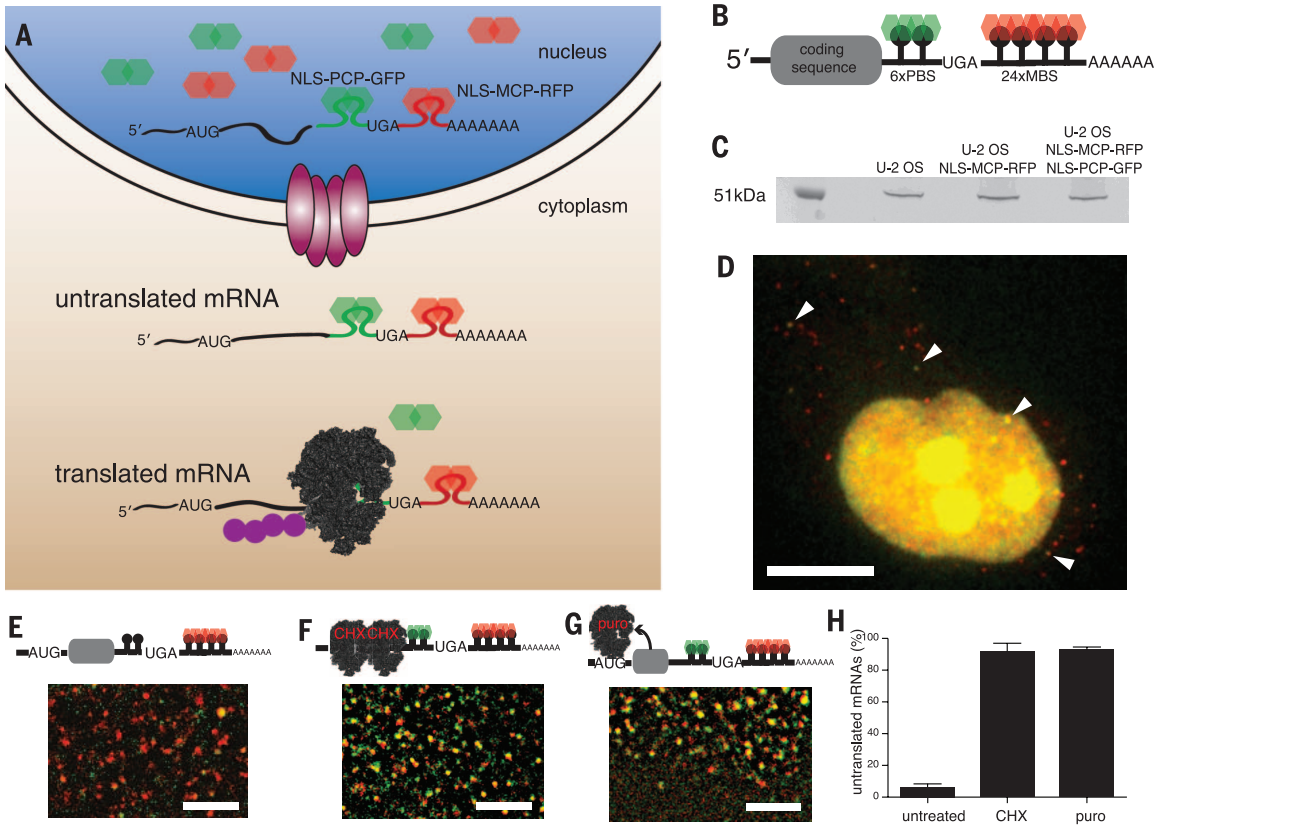

Fig. 1. Imaging translation of mRNAs in living cells. (**A**) Schematic of TRICK assay. (**B**) Schematic of TRICK reporter transcript. 6xPP7 stem-loops (PBS) inserted in-frame with the C terminus of a protein-coding sequence and 24xMS2 stem-loops (MBS) in the 3′ UTR. (**C**) Expression of TRICK reporter mRNA in U-2 OS cells. The protein encoded by the TRICK reporter (51.4 kD) is translated in U-2 OS cells, and expression is not affected by NLS-MCP-RFP and NLS-PCP-GFP. (**D**) U-2 OS cell expressing TRICK reporter. Arrows indicate untranslated nuclear mRNA and three untranslated mRNAs detected in the cytoplasm. Scale bar, 10 μm. (**E**) Cytoplasmic region of untreated U-2 OS cells. (**F**) Addition of cycloheximide (100 $\mu g\ ml^{-1}$) and (**G**) addition of puromycin (100 $\mu g\ ml^{-1}$) during ponA induction of TRICK reporter mRNAs. Scale bar (E to G), 2 μm. (**H**) Percentage of untranslated TRICK mRNAs in U-2 OS cells. In untreated cells, 5.8 ± 1.4% of mRNAs colocalize with both NLS-PCP-GFP and NLS-MCP-RFP compared to 91.0 ± 3.0% for cycloheximide-treated and 92.6 ± 1.0% for puromycin-treated cells. n = 5 cells for each condition.

diffuse away from the nucleus, their chances to collide with the 43*S* preinitiation complex and become translated increase over time. Indeed, we observed that the fraction of untranslated mRNAs decreased gradually as the distance from the nucleus increased (fig. S10C). Spatial profiles of untranslated mRNAs demonstrated that some mRNAs diffused micrometers away from the nucleus before undergoing translation, indicating that translation does not occur immediately upon export, but occurs minutes after the mRNA has entered the cytoplasm (the time before an mRNA translates should scale as L^2/D, where $L \sim 5\,\mu m$ is the radial extent of the untranslated mRNA profile and $D = 0.02$ to $0.13\ \mu m^2\ s^{-1}$ is the range of diffusion coefficients; fig. S9). Furthermore, we find no evidence for enrichment or depletion at specific cytosolic locations, suggesting that translation can occur homogeneously throughout the cytoplasm.

We next investigated how stress conditions affect translation. Upon a variety of cellular stresses, signaling pathways inhibit translation through phosphorylation of eukaryotic translation initiation factor 2α (eIF2α), resulting in disassembly of polysomes and formation of cytoplasmic stress granules and processing bodies (P-bodies), cytoplasmic organelles whose role in RNA metabolism is not well understood (*15*, *16*). The mRNAs and proteins that constitute these organelles are dynamic and rapidly exchange with the cytosol (*17*, *18*). However, mRNAs containing 5′ terminal oligopyrimidine (TOP) motifs accumulate in stress granules upon amino acid starvation, suggesting that certain mRNA classes may be differentially regulated within these compartments (*19*). To characterize the spatiotemporal regulation of 5′ TOP mRNA translation during stress, a tetracycline-inducible HeLa cell line expressing a 5′ TOP TRICK reporter mRNA with green (NLS-PCP-GFP) and red (NLS-MCP-Halo; JF_{549}) fluorescent proteins required for single-molecule RNA imaging were stressed with arsenite. 5′ TOP TRICK mRNAs were detected as single molecules distributed throughout the cytosol or located within stress granules and P-bodies. Only mRNAs sequestered within P-bodies formed large clusters. This association with P-bodies was specific for the 5′ TOP TRICK mRNAs because a reporter that lacked the 5′ TOP motif did not form multimeric assemblies within these cytoplasmic foci (Fig. 2, A to C).

To address the translational regulation of cytosolic mRNAs and those clustered in P-bodies, we induced transcription of the 5′ TOP TRICK reporter mRNA for a short period before addition of arsenite. This resulted in an increase in the number of untranslated mRNAs in the cytoplasm to be detected compared to unstressed cells, consistent with an inhibition of eIF2.GTP.Met-tRNAi^{Met} formation (Fig. 2, D and F). The untranslated 5′ TOP TRICK reporter mRNAs in the cytoplasm were detected as either single mobile mRNAs or static clusters within P-bodies. Photobleaching of the clustered mRNAs indicated that they were stably associated with P-bodies (fig. S11). Upon removal of arsenite, 5′ TOP TRICK mRNAs in the cytosol underwent translation; however, the clustered transcripts retained in P-bodies remained untranslated, indicating that these cellular structures can provide a distinct level of regulation (Fig. 2, E and F, and movies S6 to S7).

Messenger ribonucleoprotein (mRNP) granules form not only during cellular stress, but also as part of normal regulatory pathways. In *Drosophila*, localized expression of Oskar protein at the posterior pole of the oocyte is essential for correct body patterning and germ cell formation (*20*). Precise spatiotemporal translational regulation is crucial during long-range transport of *oskar* mRNA (*osk*) from the nurse cells, where the mRNA

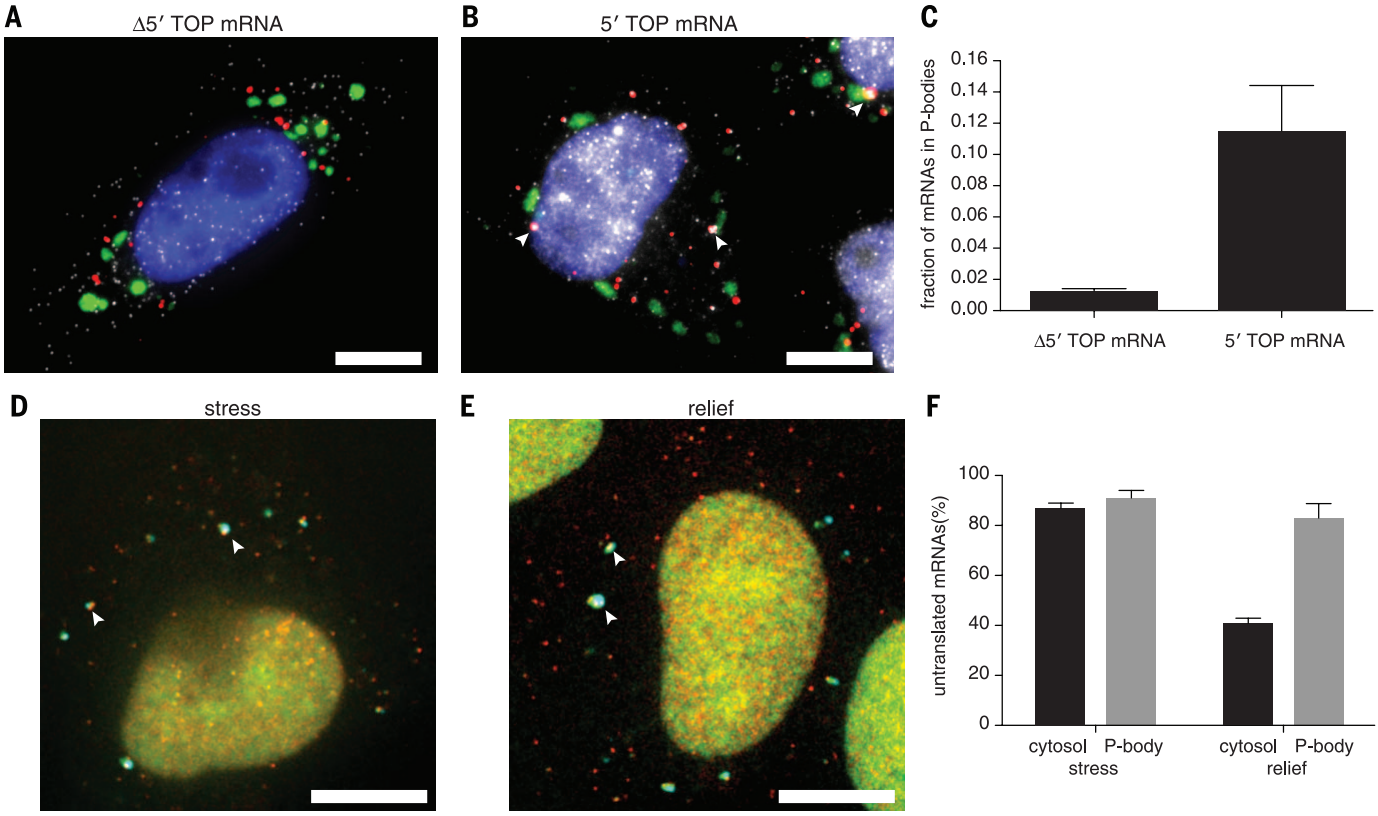

Fig. 2. P-bodies are sites of translation regulation during stress in HeLa cells. (**A** and **B**) IF-FISH of cells expressing Δ5′ TOP TRICK reporter mRNA [(A), gray] or 5′ TOP TRICK reporter mRNA [(B), gray] during arsenite stress (0.5 mM) contain stress granules (TIAR, green) and P-bodies (DDX6, red). Arrows: mRNA clusters in P-bodies. (**C**) Fraction of cytoplasmic Δ5′ TOP (n = 19 cells) and 5′ TOP (n =17 cells) mRNAs located within P-bodies after 60 min of arsenite (0.5 mM) stress (P = 0.0009, unpaired t test). (**D** and **E**) Live-cell image of 5′ TOP TRICK reporter mRNA during arsenite stress (D) and relief of stress (E). In stressed cells, mRNAs (red, green) in cytosol and P-bodies (cyan) are untranslated. In relieved cells, many mRNAs (red, green) in cytosol have been translated whereas mRNAs retained in P-bodies (cyan) remain untranslated. Arrow: clustered mRNAs. Scale bar (A, B, D, E), 10 μm. (**F**) Percentage of untranslated mRNAs (cytosol and P-bodies) during stress (n = 9 cells) and relief of stress (n = 10 cells). Upon relief of stress, 5′ TOP mRNAs in P-bodies are not translated (P = 0.31, unpaired t test); mRNAs in the cytosol have undergone translation ($P < 0.0001$, unpaired t test).

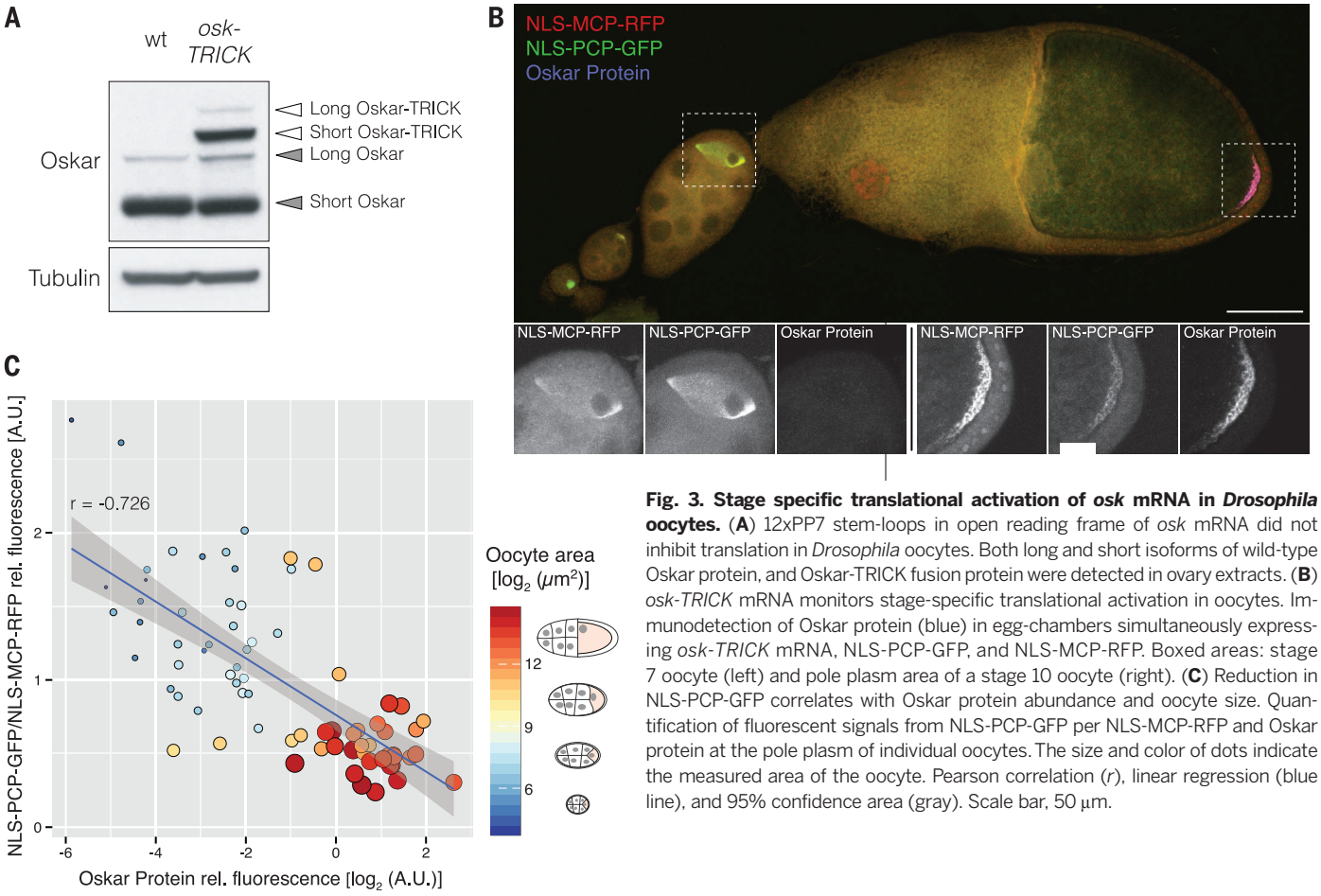

Fig. 3. Stage specific translational activation of *osk* mRNA in *Drosophila* oocytes. (**A**) 12xPP7 stem-loops in open reading frame of *osk* mRNA did not inhibit translation in *Drosophila* oocytes. Both long and short isoforms of wild-type Oskar protein, and Oskar-TRICK fusion protein were detected in ovary extracts. (**B**) *osk-TRICK* mRNA monitors stage-specific translational activation in oocytes. Immunodetection of Oskar protein (blue) in egg-chambers simultaneously expressing *osk-TRICK* mRNA, NLS-PCP-GFP, and NLS-MCP-RFP. Boxed areas: stage 7 oocyte (left) and pole plasm area of a stage 10 oocyte (right). (**C**) Reduction in NLS-PCP-GFP correlates with Oskar protein abundance and oocyte size. Quantification of fluorescent signals from NLS-PCP-GFP per NLS-MCP-RFP and Oskar protein at the pole plasm of individual oocytes. The size and color of dots indicate the measured area of the oocyte. Pearson correlation (*r*), linear regression (blue line), and 95% confidence area (gray). Scale bar, 50 μm.

is transcribed, to the posterior pole of the oocyte, where Oskar protein first appears during mid-oogenesis (stage 9) (*21*, *22*). Additional mechanisms ensure degradation of ectopically expressed Oskar protein; hence, absence of the protein does not indicate lack of translation of its mRNA (*23*).

To monitor translation, we generated an *osk*-TRICK reporter mRNA by placing 12xPP7 stem-loops within the coding region of a construct that contained 6xMS2 stem-loops in the 3′ UTR (fig. S12) (*24*). Introducing 12xPP7 stem-loops into the open reading frame of *osk* mRNA did not inhibit translation of the reporter transcript, and the fusion protein was expressed at levels comparable to that of the wild-type protein (Fig. 3A). In early-stage oocytes of flies coexpressing *osk*-TRICK mRNA, NLS-MCP-RFP, and NLS-PCP-GFP, *osk*-TRICK mRNA was labeled by both NLS-PCP-GFP and NLS-MCP-RFP, indicating translational repression consistent with the absence of Oskar protein (Fig. 3B). In later stages, the NLS-PCP-GFP fluorescent signal was reduced at the posterior pole and Oskar protein was detected by immunofluorescence, consistent with translation of a portion of the transcripts (Fig. 3, B and C). This methodology provides a framework for analyzing the cascade of regulatory mechanisms required for local translation during *Drosophila* development. It will also be informative in neurons where regulation of the first round of translation has been shown to be important for local protein synthesis in axons and dendrites (*25*, *26*).

This methodology pinpoints the precise time and place of the first translation event of single mRNA molecules. It reveals the translation control of mRNAs sequestered within cytoplasmic organelles or when and where the translation of a key cell fate determinant occurs in an organism undergoing development. The kinetics of translational regulation can now be coupled with single-molecule imaging of proteins to provide insights into mechanisms of regulation that were previously unapproachable by ensemble biochemical or genetic approaches (*27*). Observing regulation of mRNA translation in single living cells will lead to a better understanding of disease mechanisms.

REFERENCES AND NOTES

1. N. T. Ingolia, S. Ghaemmaghami, J. R. Newman, J. S. Weissman, *Science* **324**, 218–223 (2009).
2. B. Schwanhäusser *et al.*, *Nature* **473**, 337–342 (2011).
3. D. R. Larson, D. Zenklusen, B. Wu, J. A. Chao, R. H. Singer, *Science* **332**, 475–478 (2011).
4. A. Raj, A. van Oudenaarden, *Annu. Rev. Biophys.* **38**, 255–270 (2009).
5. J. A. Chao, Y. J. Yoon, R. H. Singer, *Cold Spring Harb. Perspect. Biol.* **4**, a012310 (2012).
6. S. Hocine, P. Raymond, D. Zenklusen, J. A. Chao, R. H. Singer, *Nat. Methods* **10**, 119–121 (2013).
7. M. K. Doma, R. Parker, *Nature* **440**, 561–564 (2006).
8. D. No, T. P. Yao, R. M. Evans, *Proc. Natl. Acad. Sci. U.S.A.* **93**, 3346–3351 (1996).
9. K. Al-Jubran *et al.*, *RNA* **19**, 1669–1683 (2013).
10. A. David *et al.*, *J. Cell Biol.* **197**, 45–57 (2012).
11. Y. Shav-Tal *et al.*, *Science* **304**, 1797–1800 (2004).
12. A. Mor *et al.*, *Nat. Cell Biol.* **12**, 543–552 (2010).
13. C. P. Stanners, *Biochem. Biophys. Res. Commun.* **24**, 758–764 (1966).
14. T. Trcek, H. Sato, R. H. Singer, L. E. Maquat, *Genes Dev.* **27**, 541–551 (2013).
15. J. R. Buchan, R. Parker, *Mol. Cell* **36**, 932–941 (2009).
16. N. Kedersha, P. Ivanov, P. Anderson, *Trends Biochem. Sci.* **38**, 494–506 (2013).
17. N. Kedersha *et al.*, *J. Cell Biol.* **169**, 871–884 (2005).
18. S. Mollet *et al.*, *Mol. Biol. Cell* **19**, 4469–4479 (2008).
19. C. K. Damgaard, J. Lykke-Andersen, *Genes Dev.* **25**, 2057–2068 (2011).
20. A. Ephrussi, R. Lehmann, *Nature* **358**, 387–392 (1992).
21. J. Kim-Ha, K. Kerr, P. M. Macdonald, *Cell* **81**, 403–412 (1995).
22. F. H. Markussen, A. M. Michon, W. Breitwieser, A. Ephrussi, *Development* **121**, 3723–3732 (1995).
23. E. Morais-de-Sá, A. Vega-Rioja, V. Trovisco, D. St Johnston, *Dev. Cell* **26**, 303–314 (2013).
24. M. D. Lin *et al.*, *Dev. Biol.* **322**, 276–288 (2008).
25. D. Colak, S. J. Ji, B. T. Porse, S. R. Jaffrey, *Cell* **153**, 1252–1265 (2013).
26. C. Giorgi *et al.*, *Cell* **130**, 179–191 (2007).
27. M. E. Tanenbaum, L. A. Gilbert, L. S. Qi, J. S. Weissman, R. D. Vale, *Cell* **159**, 635–646 (2014).

ACKNOWLEDGMENTS

This was work supported by the Novartis Research Foundation (J.A.C); NIH grants NS83085, EB013571, and GM57071 (R.H.S); Howard Hughes Medical Institute (R.H.S and T.L.); European Molecular Biology Laboratory (EMBL) (A.E.); and a postdoctoral fellowship from the EMBL Interdisciplinary Postdoc Program (EIPOD) under Marie Curie COFUND actions (F.W.). We thank C. Damgaard (University of Aarhus) for providing the rpL32-

β-globin plasmid; S. Shenoy (Albert Einstein College of Medicine), L. Gelman and S. Bourke (Friedrich Miescher Institute), and EMBL Advanced Light Microscopy Facility for microscopy support; D. Ciepielewski (Nikon) for providing access to NIS tracking software; C. Eliscovich (Albert Einstein College of Medicine) for advice on IF-FISH; L. Lavis (Janelia Farm) for providing JF_{549} dye; M. Beal (Biosearch Technologies) for Stellaris FISH probes; A. Arnold (FMI) for assistance with polysome analysis; I. Gáspár (EMBL) for pHsp83 vector; and S. Chao, U. Meier, and J. Warner for helpful discussions.

SUPPLEMENTARY MATERIALS

www.sciencemag.org/content/347/6228/1367/suppl/DC1
Materials and Methods
Figs. S1 to S12
Movies S1 to S7
References (*28*–*37*)

20 November 2014; accepted 6 February 2015
10.1126/science.aaa3380

RNA BIOCHEMISTRY

Determination of in vivo target search kinetics of regulatory noncoding RNA

Jingyi Fei,[1] Digvijay Singh,[2] Qiucen Zhang,[1] Seongjin Park,[1] Divya Balasubramanian,[3] Ido Golding,[1,4] Carin K. Vanderpool,[3]* Taekjip Ha[1,2,5,6]*

Base-pairing interactions between nucleic acids mediate target recognition in many biological processes. We developed a super-resolution imaging and modeling platform that enabled the in vivo determination of base pairing–mediated target recognition kinetics. We examined a stress-induced bacterial small RNA, SgrS, which induces the degradation of target messenger RNAs (mRNAs). SgrS binds to a primary target mRNA in a reversible and dynamic fashion, and formation of SgrS-mRNA complexes is rate-limiting, dictating the overall regulation efficiency in vivo. Examination of a secondary target indicated that differences in the target search kinetics contribute to setting the regulation priority among different target mRNAs. This super-resolution imaging and analysis approach provides a conceptual framework that can be generalized to other small RNA systems and other target search processes.

Base-pairing interactions between nucleic acids constitute a large category of target recognition processes such as noncoding RNA-based gene regulation [e.g., microRNAs (*1*) and long noncoding RNAs (*2*) in eukaryotes and small RNAs (sRNAs) in bacteria (*3*)], bacterial adaptive immunity [e.g., the clustered regularly interspaced short palindromic repeat (CRISPR) system (*4*)], and homologous recombination (*5*). Although target search kinetics by transcription factors has been studied in vivo (*6*), the rate constants for target identification via base-pairing interactions in vivo are not known for any system. Here, we developed a super-resolution imaging and analysis platform to assess the kinetics of base-pairing interaction-mediated target recognition for a bacterial sRNA, SgrS. SgrS is produced upon sugar-phosphate stress, and its function is dependent on an RNA chaperone protein Hfq. SgrS regulates several target mRNAs posttranscriptionally through base-pairing interactions that affect mRNA translation and stability (*7*). We combined single-molecule fluorescence in situ hybridization (smFISH) (*8*) with single-molecule localization-based super-resolution microscopy (*9*) to count RNAs and obtain information on subcellular localization. High spatial resolution is required for accurate quantification of the high-copy-number RNAs and sRNA-mRNA complexes. Here, simultaneous measurements of sRNA, mRNA, and sRNA-mRNA complexes together with mathematical modeling allow determination of key parameters describing sRNA target search and downstream codegradation of sRNA-mRNA complexes.

We first studied the kinetic properties of SgrS regulation of *ptsG* mRNA, encoding a primary glucose transporter. SgrS binds within the 5′ untranslated region (UTR) of *ptsG* mRNA, blocks its translation, and induces its degradation (*10*). We induced stress and SgrS production in *Escherichia coli* strains derived from wild-type MG1655 (table S1) using a nonmetabolizable sugar analog, α-methyl glucoside (αMG) (*10*, *11*). Fractions of cell culture were taken at different time points after induction and fixed (*12*). Oligonucleotide probes (table S2) labeled with photoswitchable dyes, Alexa 647 and Alexa 568, were used to detect SgrS (9 probes) and *ptsG* mRNA (28 probes), respectively, using smFISH (*8*). We then imaged the cells using two-color three-dimensional (3D) super-resolution microscopy (*9*, *12*) (Fig. 1A; compare to diffraction limited images in Fig. 1B).

In the wild-type strain (table S1), we observed production of SgrS and corresponding reduction of *ptsG* mRNA over a few minutes (Fig. 1A), consistent with SgrS-mediated degradation of *ptsG* mRNA (*10*). In a strain producing an SgrS that does not base pair with *ptsG* mRNA due to mutations in the seed region (*13*, *14*) and in an Hfq deletion (Δ*hfq*) strain (table S1), *ptsG* mRNA reduction was not observed (figs. S1 and S2). To quantify the copy number of RNAs in each cell, we employed a density-based clustering algorithm to map single-molecule localization signal to individual clusters corresponding to individual RNAs (*12*, *15*, *16*) (Fig. 1C and movies S1 and S2). The absolute copy number quantification was validated by quantitative polymerase chain reaction (qPCR) (*12*) (Fig. 1D).

We next built a kinetic model containing the following kinetic steps: transcription of SgrS (with rate constant α_S) and *ptsG* (α_p), endogenous degradation of *ptsG* mRNA (with rate constant β_p), degradation of SgrS in the absence of codegradation with *ptsG* mRNA ($\beta_{S,p}$), binding of SgrS to *ptsG* mRNA (with rate constant k_{on}), dissociation of SgrS from *ptsG* mRNA (k_{off}), and ribonuclease E (RNase E)–mediated codegradation of SgrS-*ptsG* mRNA complex (k_{cat}) (Fig. 1E). We independently measured β_p and the total SgrS degradation rate, including endogenous and mRNA-coupled degradation [table S4, fig. S3, and supplementary materials section 1.9 (SM 1.9)]. Because *ptsG* mRNA levels remained constant in the absence of SgrS-mediated degradation, as observed in the base-pairing mutant strain (fig. S1), we determined α_p as the product of β_p and *ptsG* mRNA concentration before SgrS induction (table S4 and SM 1.10)

To determine k_{on} and k_{off}, it is necessary to count the SgrS-*ptsG* mRNA complexes. Colocalization of *ptsG* mRNA and SgrS at the 40-nm resolution was rarely observed in the wild-type strain (up to ~5%, similar to ~3% colocalization by chance, estimated using the base-pairing mutant as a negative control) (Fig. 2). This is possibly because SgrS regulates several other target mRNAs (*7*) and/or the SgrS-*ptsG* mRNA complex may be unstable due to rapid codegradation or disassembly. In an RNase E mutant strain, in which codegradation is blocked (*17*, *18*) (table S1), *ptsG* mRNA levels stayed the same as SgrS levels increased (fig. S4) (*17*, *18*), and a fraction of *ptsG* mRNA colocalized with SgrS, increasing over time to reach ~15% (Fig. 2 and fig. S5). A positive control using *ptsG* mRNA simultaneously labeled with two colors (Fig. 2 and SM 1.8) showed a high degree of colocalization (~70%), similar to the reported detection efficiency of colocalization by super-resolution imaging (*19*).

We then applied these measured parameters (α_p and β_p), used total SgrS degradation rate as a constraint for $\beta_{S,p}$, and determined the remaining parameters (α_S, $\beta_{S,p}$ k_{on}, k_{off}, and k_{cat}) by fitting equations (Fig. 1E) to the six time-course changes of SgrS, *ptsG* mRNA, and SgrS-*ptsG* mRNA complex in both the wild-type and the RNase E mutant strains (Fig. 3A, table S4, and SM 1.10). We further validated the model by changing

[1]Center for the Physics of Living Cells, Department of Physics, University of Illinois, Urbana, IL, USA. [2]Center for Biophysics and Computational Biology, University of Illinois, Urbana, IL, USA. [3]Department of Microbiology, University of Illinois, Urbana, IL, USA. [4]Verna and Marrs McLean Department of Biochemistry and Molecular Biology, Baylor College of Medicine, Houston, TX, USA. [5]Carl R. Woese Institute for Genomic Biology, Howard Hughes Medical Institute, Urbana, IL, USA. [6]Howard Hughes Medical Institute, Urbana, IL, USA.
*Corresponding author. E-mail: tjha@illinois.edu (T.H.); cvanderp@life.uiuc.edu (C.K.V.)